Research paper

Synthesis, pharmacology and preclinical evaluation of ^{11}C-labeled 1,3-dihydro-2*H*-benzo[d]imidazole-2-ones for imaging γ8-dependent transmembrane AMPA receptor regulatory protein

Zhen Chen [a, b, 1], Wakana Mori [c, 1], Xiaofei Zhang [a], Tomoteru Yamasaki [c], Patrick J. Dunn [d], Genwei Zhang [e], Hualong Fu [a], Tuo Shao [a], Yiding Zhang [c], Akiko Hatori [c], Longle Ma [a], Masayuki Fujinaga [c], Lin Xie [c], Xiaoyun Deng [a], Hua Li [a], Qingzhen Yu [a], Jian Rong [a], Lee Josephson [a], Jun-An Ma [b], Yihan Shao [e], Susumu Tomita [d], Ming-Rong Zhang [c, **], Steven H. Liang [a, *]

[a] *Division of Nuclear Medicine and Molecular Imaging, Massachusetts General Hospital & Department of Radiology, Harvard Medical School, Boston, MA, 02114, USA*
[b] *Department of Chemistry, School of Science, Tianjin University, 92 Weijin Road, Nankai District, Tianjin 300072, China*
[c] *Department of Radiopharmaceutics Development, National Institute of Radiological Sciences, National Institutes for Quantum and Radiological Science and Technology, Chiba, 263-8555, Japan*
[d] *Department of Cellular and Molecular Physiology, Department of Neuroscience, Yale University School of Medicine, New Haven, CT, USA*
[e] *Department of Chemistry and Biochemistry, University of Oklahoma, Norman, OK, 73019, USA*

ARTICLE INFO

ABSTRACT

a-Amino-3-hydroxyl-5-methyl-4-isoxazolepropionic acid (AMPA) receptors are implicated in the pathology of neurological diseases such as epilepsy and schizophrenia. As pan antagonists for this target are often accompanied with undesired effects at high doses, one of the recent drug discovery approaches has shifted to subtype-selective AMPA receptor (AMPAR) antagonists, specifically, via modulating transmembrane AMPAR regulatory proteins (TARPs). The quantification of AMPARs by positron emission tomography (PET) would help obtain insights into disease conditions in the living brain and advance the translational development of AMPAR antagonists. Herein we report the design, synthesis and preclinical evaluation of a series of TARP γ-8 antagonists, amenable for radiolabeling, for the development of subtype-selective AMPAR PET imaging agents. Based on the pharmacology evaluation, molecular docking studies and physiochemical properties, we have identified several promising lead compounds **3**, **17**–**19** and **21** for *in vivo* PET studies. All candidate compounds were labeled with [^{11}C]COCl$_2$ in high radiochemical yields (13–31% RCY) and high molar activities (35–196 GBq/μmol). While tracers **30** ([^{11}C]**17**) & **32** ([^{11}C]**21**) crossed the blood-brain barrier and showed heterogeneous distribution in PET studies, consistent with TARP γ-8 expression, high nonspecific binding prevented further evaluation. To our delight, tracer **31** ([^{11}C]**3**) showed good *in vitro* specific binding and characteristic high uptake in the hippocampus in rat brain tissues, which provides the guideline for further development of a new generation subtype selective TARP γ-8 dependent AMPAR tracers.

© 2018 Elsevier Masson SAS. All rights reserved.

1. Introduction

As the primary excitatory neurotransmitter in the mammalian brain, glutamate exerts postsynaptic effects through a diversity of metabotropic and ionotropic receptors (mGluRs and iGluRs, respectively) [1,2]. In particular, iGluRs are glutamate-gated tetrameric ion channels. Based on their preferential ligands they can be further divided into three main categories, namely *a*-amino-3-
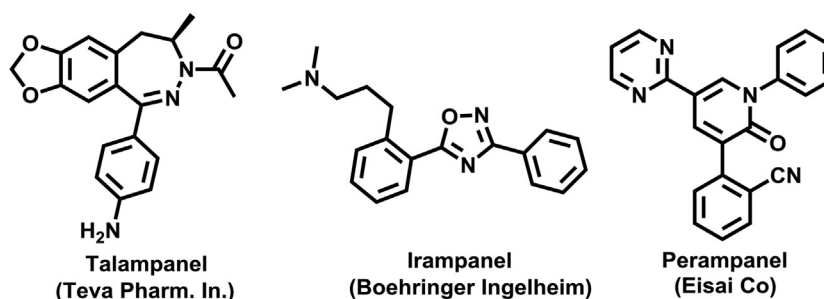
hydroxyl-5-methyl-4-isoxazolepropionic acid (AMPA) receptors, *N*-methyl-*d*-aspartate (NMDA) receptors, and kainate receptors [3–6]. The AMPA receptors (AMPARs) are primarily expressed on post-synaptic membranes of excitatory synapses and regulate fast synaptic transmission in the central nervous system (CNS) [7]. AMPARs play a significant role in memory and learning [3], and are also implicated in the etiology of several excitotoxic diseases such as epilepsy and ischemia [8,9]. As a potential therapeutic target, early pharmacotherapies for CNS disorders caused by excessive neuronal activity have focused on pan AMPAR antagonists, including fana-panel [10], becampanel [11], tezampanel [12], selurampanel [13], talampanel [14], irampanel [15], and perampanel [16–18]. Per-ampanel (Fycompa™; Fig. 1A) has been approved by the US Food and Drug Administration (FDA). Since AMPARs are expressed ubiquitously in the CNS, these pan antagonists are often accompanied with undesired effects at high doses, such as dizziness, ataxia, and sedation [17]. To address these challenges, researchers have shifted their therapeutic approach to a new strategy utilizing subtype-selective AMPAR antagonists, specifically, via modulating transmembrane AMPAR regulatory proteins (TARPs) [19–21]. As a recently discovered family of receptor auxiliary subunits [22–24], TARPs have been found to associate with and regulate AMPAR trafficking, gating, protein levels as well as pharmacology [25–27]. TARPs are categorized into two subgroups based on their sequence homology, group I (γ-2/stargazin, γ-3, γ-4, and γ-8) and group II (γ-5, γ-7). Several TARPs are found to be distributed in the brain in a regiospecific manner [28,29], such as cerebellum-enriched TARP γ-2 and hippocampus-enriched TARP γ-8, highlighting the feasibility of selective regulation of AMPAR activity in specific brain circuits by targeting individual TARP subtypes without the aforementioned side effects [30]. In particular, TARP γ-8 antagonism is especially promising for the development of therapies for pathologic disorders distinguished by hyperactivity within forebrain [31–34]. It is encouraging that there are several TARP γ-8-dependent antagonists including JNJ55511118 [35] and LY3130481 [36–38] debuted in late 2016, among which LY3130481 has been advanced to phase I

clinical trial in 2017 (Fig. 1B).

As a non-invasive imaging technology, positron emission tomography (PET) is ideal for *in vivo* quantification of biochemical and pharmacological process under both normal and disease conditions with minimal perturbation of the original biological state [39–41]. PET imaging studies of AMPARs in the living brain would help to obtain insights into excitotoxic conditions and to advance the translational development of AMPAR antagonists via target engagement studies, as well as to enable pharmacokinetic profiling of candidate drug molecules. Despite the fact that several AMPAR PET tracers [42–45] have been developed including [11C]HMS011 [46,47] and our [18F] perampanel analog (Fig. 2A) [48], further improvement on target:nonspecific binding ratio is necessary for clinical research[47]. Furthermore, there is no subtype-selective AMPAR PET tracer (i.e., regulated via specific TARP subgroup) available for drug discovery and translational human imaging studies, despite their advantage of significantly reduced side effects over traditional pan AMPAR antagonists. As a result, the unmet clinical need of TARP γ-8 selective AMPAR PET tracers, together with the therapeutic potential of TARP γ-8 modulating pharmacotherapy, provides a strong stimulus to advance PET tracer development for this target.

As part of our continuing interest in the development of AMPAR-targeting PET tracers [48], we presented herein a novel class of TARP γ-8 dependent AMPAR PET tracers. Our medicinal chemistry efforts concentrated on the synthesis of a focused array of 1,3-dihydro-2*H*-benzo [*d*]imidazole-2-ones and benzo [*d*]thiazol-2(3*H*)-ones based on recently discovered JNJ5551118 scaffold [35]. These molecules are amenable for radiolabeling with carbon-11 or fluorine-18 for PET imaging studies (Fig. 2B). Preliminary pharmacology, molecule docking studies and physicochemical properties evaluation of top candidates were carried out to select the most promising γ-8 dependent TARP antagonists **3**, **17**–**19** and **21** for *in vivo* evaluation using PET. Utilizing [11C]COCl2 labeling strategy, we first evaluated brain permeability and specificity of candidate compounds by PET and *in vitro* autoradiography studies. We also

A. Pan AMPAR antagonist

Talampanel
(Teva Pharm. In.)

Irampanel
(Boehringer Ingelheim)

Perampanel
(Eisai Co)

B. TARP γ8-dependent AMPAR antagonists

JNJ-55511118
(Janssen)

LY3130481
(Eli Lilly)
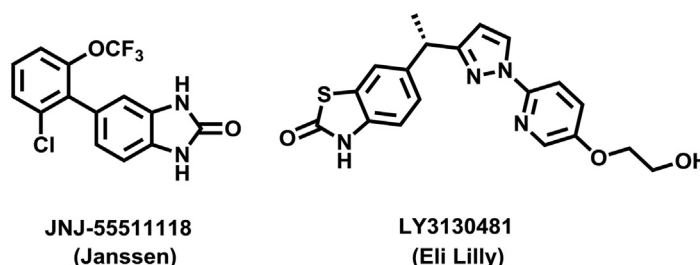
Fig. 1. Representative AMPAR antagonists.
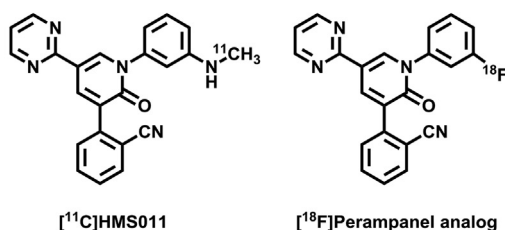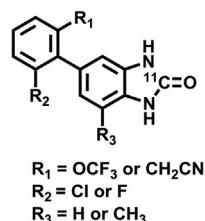
Fig. 2. Representative AMPAR PET tracers.

unveiled the underlying cause of low brain penetration for **31**, the most *in vitro* specific tracer in our design, which provides a medicinal chemistry roadmap for future design of TARP γ-8 dependent AMPAR antagonists and PET tracers.

2. Results and discussion

2.1. Chemistry

A focused library of 1,3-dihydro-2*H*-benzo [d]imidazole-2-ones **3**, **17**–**24** and benzo [d]thiazol-2(3*H*)-ones **27**–**29** were synthesized with emphasis on amenability for radiolabeling with carbon-11 or fluorine-18. As summarized in Scheme 1, initial attempt on direct palladium-catalyzed cross-coupling of (2-oxo-2,3-dihydro-1*H*-benzo [d]imidazole-5-yl)borate **1** with 2-(3-chloro-2-iodophenyl) acetonitrile **2** offered the desired urea-type AMPAR inhibitor **3** in low yield (<10%). Fortunately, when (4-amino-3-nitrophenyl) borate **4** was employed as the starting material, its cross-coupling with **2** followed by Fe-mediated reduction readily generated [1,1′-biaryl]-3,4-diamine **5** in 67% yield over two steps, which served as an important precursor for subsequent 11C-labeling. The cyclization of diamine **5** was achieved by reacting with 1,1′-carbonyldiimidazole (CDI) to provide the desired candidate **3** in 90% yield. Another [1,1′-biaryl]-3,4-diamine **9** was also obtained in 46% yield via an analogous two-step sequence of palladium-catalyzed coupling of aryl boric acid **6** with 4-bromo-2-nitroaniline **7** followed by Fe-mediated reduction. However, further studies demonstrated that direct cross-coupling between aryl boric acid **6** and 4-bromobenzene-1,2-diamines **8** represented a more efficient and step-economical avenue, thus delivering [1,1′-biaryl]-3,4-diamines **9**–**16** in good to excellent yields (42–85%). Subsequent cyclization triggered by CDI smoothly occurred to give the urea-type AMPAR antagonists **17**–**24** in 52–82% yields. The carbamothioate-type AMPAR inhibitors **27**–**29** were obtained in 62–83% yields through protection of 6-bromobenzo [d]thiazol-2(3*H*)-one **25** with Boc₂O, followed by the cross-coupling reactions with aryl boric acid **6**. It was worth noting that Boc-protected thiazlolone intermediate **26** is critical for the high-yielding (62–83%) cross-coupling reactions with **6** since merely 5% yield was observed when using unprotected **25**.

2.2. Pharmacology

Compounds **3**, **17**–**24** and **27**–**29** were subsequently screened for their *in vitro* potency and selectivity towards AMPARs associated with TARP γ-8. The results are shown in Fig. 3. Since GluA1 subunit is one of the major AMPARs expressed in hippocampus, we utilized GluA1 as the principal AMPAR subunit in our *in vitro* pharmacological studies. The splice variant flop isoform of GluA1 was used in our assay due to its faster desensitization than the flip isoform and

increased modulation by TARP. Specifically, an intracellular calcium flux system in human embryonic kidney 293 (HEK-293) cells expressing AMPA receptor GluA1o fusion construct with TARP γ-8 or γ-2 was used to evaluate the ability of candidate compound to block glutamate-induced increases using fluorescence imaging plate reader (FLIPR)-based assays. With these *in vitro* assays in place, based on a preliminary screening of antagonists at a single concentration (300 nM), urea-type compounds **3**, **17**–**19** and **21** demonstrated promising *in vitro* potency towards AMPARs associated with TARP γ-8 (as top 40% most potent compounds), while carbamothioate-type compounds **27**–**29** showed inferior potency towards TARP (Fig. 3A). Subsequently, candidate compounds **3**, **17**–**19** and **21** were determined as the IC₅₀ values for inhibition of glutamate-evoked currents in HEK293 cells co-expressing GluA1 and TARP γ-8 via concentration-response curves. All these five candidates potentially blocked human GluA1 + TARP γ-8 with IC₅₀ values as 19.5 nM for **3**, 235.3 nM for **17**, 90.9 nM for **18**, 103.3 nM for **19**, 42.6 nM for **21**, respectively (Fig. 3B). As proof of concept, we evaluated these five compounds **3**, **17**–**19** and **21** in TARP sub-type selectivity. No significant inhibition of GluA1 with TARP γ-2 was observed up to a concentration of 1 μM (Fig. 3C). Notably, no substantial off-target binding of **3** and **17** was identified in a panel of 52 receptors, ion channels and transporters, demonstrating greater than 100 fold selectivity against all tested targets [35].

2.3. Homology model and molecular docking studies

We investigated the molecular interactions of candidate antagonists with TARP γ-8 by molecular docking studies. The goal is to identify the possible key molecular interaction between TARP γ-8 antagonists and the binding domain based on the fact that nanomolar potency (19–235 nM) was determined from compounds **3**, **17**–**19** and **21**. Homology modeling-based server, SWISS-MODEL, was used to generate the three-dimensional structure of TARP γ-8, with the best hit, PDB ID 5KK2, chosen as the building template. 5KK2, a TARP γ-2, shares 48% sequence similarity with TARP γ-8 query sequence [49]. The built γ-8 model was uploaded to PDBsum and analyzed with PROCHECK program. All-residue Ramachandran plot showed that 81.9% of the residues fell into most favored regions and 17.5% of the residues fell into additional allowed regions (Fig. S1, Supporting Information). Of note is the Asp110 residue, which appeared in the disallowed region, but its corresponding Phi-Psi torsion angle was edged to an additional allowed region. The overall G-factor average of the structure was −0.26, indicating good normality. Analyzing the secondary structures of the computed TARP γ-8 model, we found four major helices, which are bundled into a trans-membrane structure (Fig. 4A) similar to the cryo-EM γ-2 structure [50], two long loops and three beta strands between transmembrane helix 1 (TM1) and TM2, as well as one loop between TM3 and TM4 (Fig. 4B). It is noteworthy that about
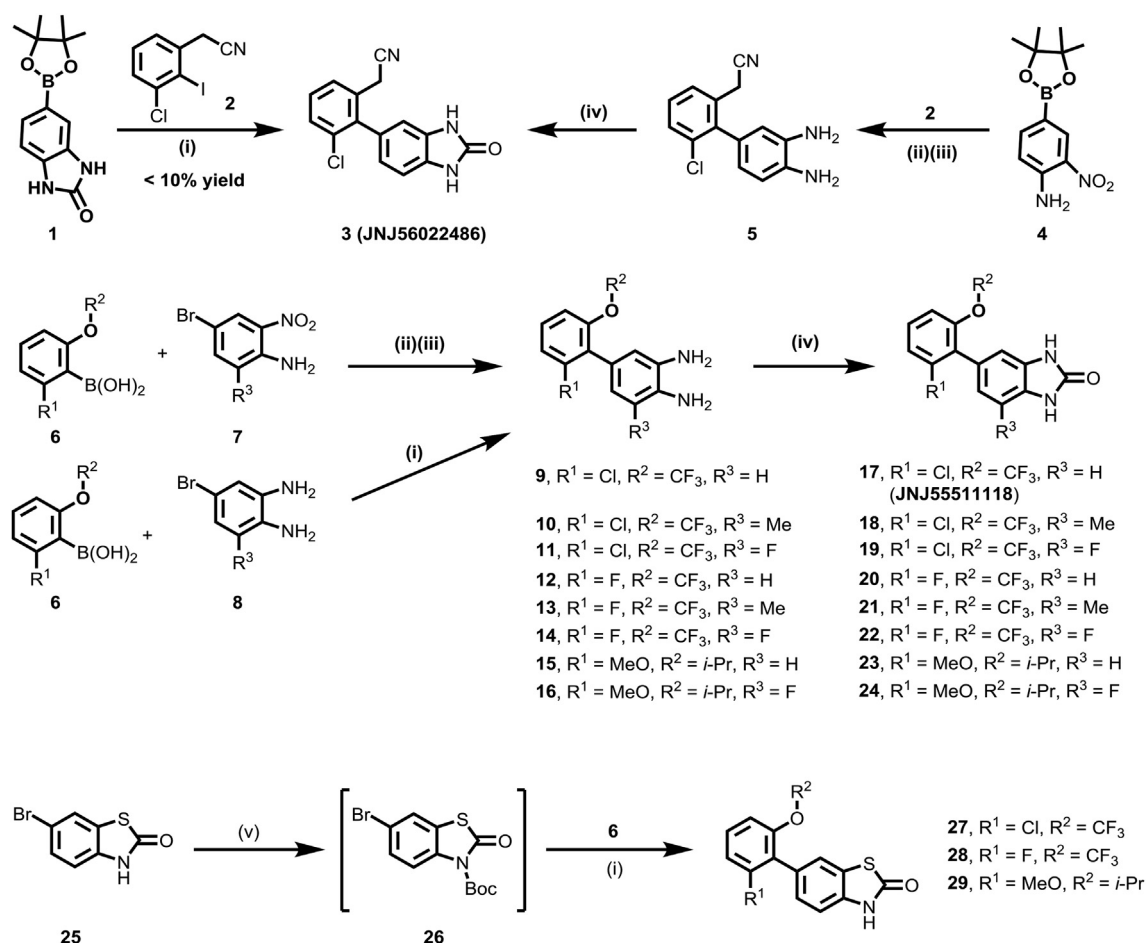
Scheme 1. Synthesis of TARP γ8-dependent AMPAR antagonists. Conditions: (i) PdCl$_2$(dtbpf), K$_3$PO$_4$, 1,4-dioxane/H$_2$O, 100 °C, 2 h; <10% yield for **3**; 53% yield for **9**; 74% yield for **10**; 86% yield for **11**; 42% yield for **12**; 46% yield for **13**; 75% yield for **14**; 66% yield for **15**; 85% yield for **16**; 62% yield for **27** over two steps; 83% yield for **28** over two steps; 78% yield for **29** over two steps; (ii) PdCl$_2$(dppf), Na$_2$CO$_3$, 1,4-dioxane/H$_2$O, 80 °C, 16 h; (iii) Fe, conc. HCl, EtOH/H$_2$O, reflux for 2 h; 67% yield for **5** over two steps; 46% yield for **9** over two steps; (iv) CDI, THF, rt, 16 h; 90% yield for **3**; 68% yield for **17**; 52% yield for **18**; 64% yield for **19**; 78% yield for **20**; 67% yield for **21**; 63% yield for **22**; 63% yield for **23**; 82% yield for **24**; (v) (Boc)$_2$O, NaH, DMF, rt, 2 h dtbpf = 1,1′-bis(di-*tert*-butylphosphino)ferrocene; dppf = 1,1′-bis(diphenylphosphino)ferrocene; DMF = *N,N*-dimethylformamide; CDI = 1,1′-carbonyldiimidazole; (Boc)$_2$O = di-tert-butyl dicarbonate.
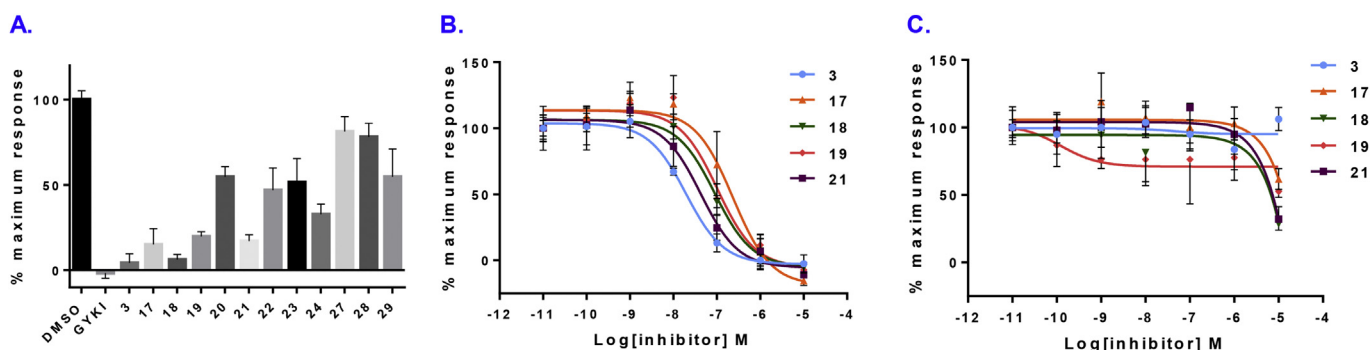

Fig. 3. Inhibition of TARP γ−8-dependent AMPAR activity by antagonists. GluA1 and TARP γ-8 were co-expressed in HEK293 cells and stimulated by glutamate and cyclothiazide. Maximal inhibition was defined by the noncompetitive AMPAR antagonist GYKI53655. A) Inhibition by 300 nM candidate compounds. B) Dose-response curves of **3**, **17**−**19** and **21** for inhibition of AMPA TARP γ-8. IC$_{50}$ values were 19.5 nM (**3**), 235.3 nM (**17**), 90.9 nM (**18**), 103.3 nM (**19**), and 42.6 nM (**21**). C) Dose-response curves of **3**, **17**−**19** and **21** for inhibition of AMPA TARP γ-2.

180 amino acids towards the TARP γ-8 C-terminus were not included in the computed model due to lacking the corresponding regions within the template; however, the missing C-terminal residues should be located within the cytoplasm [50], thus unlikely influencing the subsequent ligand docking results.

Candidate compounds, **3**, **17**−**19** and **21** were docked onto the homology-computed AMPAR/TARPγ-8 structure using Autodock Vina in Chimera [51]. Based on the docking studies, a consensus binding pocket was found within the extracellular opening of the four helices bundle, which is adjacent to TM2, TM3 and the β3-TM2
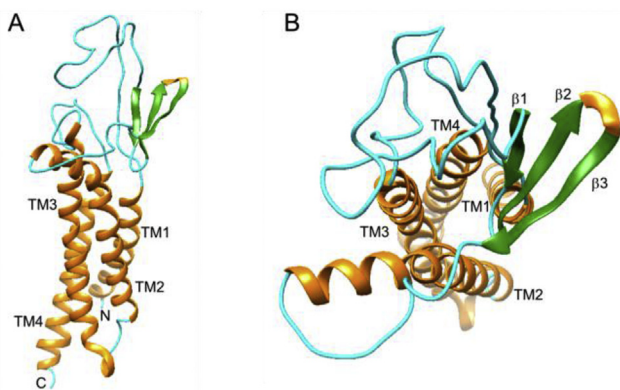
Fig. 4. Homology model of TARP γ-8. (A) Viewed parallel to the membrane; (B) Viewed from the extracellular side of the membrane.

loop (Fig. 5A). For each compound, the docking pose with the highest docking score was chosen for subsequent analyses and comparison with our experimental data. Deep into the binding pocket, an angled π-π stacking interaction was found between γ-8 Phe107 side chain and the phenyl group of the compounds (Fig. 5B). In addition, the trifluoromethoxy moiety of the compounds was found in proximity to the Lys103 side chain, indicating possible electrostatic interactions between the two. Furthermore, the side chain of Ser182 was approximately 3 Å away from one of the secondary amines of the compounds, suggesting the potential formation of a hydrogen bond.

We note that Lys103 and Phe107 belong to a highly conserved sequence (**K**INHF**P**EDTDYDHD), which was previously found across all type of TARPs [52,53], including γ-2, γ-3, γ-4 and γ-8. This conserved electronegative sequence was reported to be responsible for altering AMPAR gating and pharmacology [52,54—58]. For instance, this motif within γ-2 interacts with subunits B and D of GluA2 AMPAR [50]. Interestingly, in our study, we found the above conserved sequence within the β3-TM2 loop of the predicted TARP γ-8 structure and located next to our proposed binding pocket. This allows two of the residues, Lys103 and Phe107, to interact with the candidate compounds. Therefore, we hypothesized that binding to the candidate compounds might cause some conformational changes of the TARP γ-8 β3-TM2 loop, and consequently, interfere with the interactions between AMPAR and γ-8.

2.4. Physicochemical property

We used candidate compounds' lipophilicity as one of the predictive factors for blood-brain barrier permeability with a favorable range between 1.0 and 3.5 [59—61]. Using liquid-liquid partition
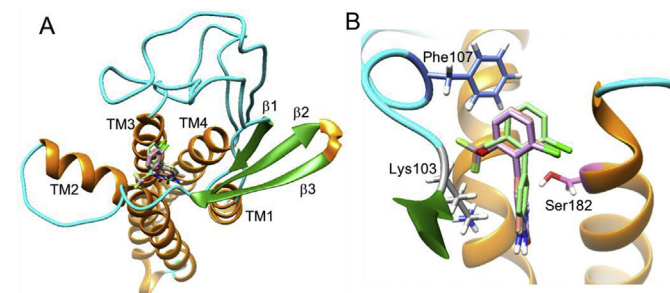

Fig. 5. Interactions between TARP γ-8 and candidate compounds **3**, **17**—**19** and **21**. A) The overview of the docking pose of the candidate compounds **3**, **17**—**19** and **21** onto TARP γ-8, and B) the zoom-in view of potential interacting residues of TARP γ-8 with the candidate compounds.

between *n*-octanol and PBS ('shake flask method') [62], the logD values of **3**, **17**—**19** and **21** were determined to be 2.13, 2.17, 2.67, 2.01 and 3.18, respectively ($n = 3$), indicating a high possibility of brain penetration (Table 1). We also utilized *in silico* prediction methods to determine the topological polar surface area (tPSA) and multiple parameter optimization (MPO) scores. The candidate compounds **3**, **17**—**19** and **21** showed a reasonable range in tPSA and MPO values as potential brain penetrant leads (Table 1). These results indicated the high possibility of sufficient brain permeability of compounds **3**, **17**—**19** and **21**. Together with binding potency, molecular docking and physicochemical properties, we chose AMPAR antagonists **3**, **17**—**19** and **21** for radiolabeling experiments.

2.5. Radiochemistry

The chemical scaffold of 1,3-dihydro-2*H*-benzo [d]imidazole-2-ones offers a unique opportunity and unified labeling strategy using ^{11}C-carbonylation methodology [64]. Dolle and Kassiou *et al.* have demonstrated the use of [^{11}C]COCl$_2$ (generated from [^{11}C]CO$_2$) to radiolabel the carbonyl position of chemical structures including 1,3-dihydrobenzoimidazol-2-one [65] and 3*H*-benzoxazol-2-one [66], respectively. Thus we adopted their methodology to carry out radiosynthesis of **30**—**33** from the corresponding precursors **9**, **5**, **13** and **10**, respectively. The [1,1′-biaryl]-3,4-diamines **5**, **9**—**10** and **13** for ^{11}C-carbonylation were synthesized by the method outlined in Scheme 2. The radiosynthesis of **30** ([^{11}C]**17**) was performed using [^{11}C]COCl$_2$ generated from our modified procedure [67] (Scheme 2A). Specifically, the reaction of [^{11}C]COCl$_2$ with benzenediamine **9** generated ^{11}C-labeled cyclic urea **17** in the presence of triethylamine (Et$_3$N) in THF. The reaction mixture was purified by a reverse phase semi-preparative HPLC, and reformulated for imaging study. **30** was synthesized in an average of 28% decay-corrected radiochemical yield (RCY) based on starting [^{11}C] CO$_2$ at end-of-synthesis with >99% radiochemical purity ($n = 2$). The molar activity was greater than 35 GBq/μmol (0.95 Ci/μmol). In an analogous fashion, **31** ([^{11}C]**3**, Scheme 2B) and **32** ([^{11}C]**21**, Scheme 2C) were radiolabeled with [^{11}C]COCl$_2$ in a range of 19—31% RCY (decay corrected) with high radiochemical purity (>99%) and high molar activity (A$_m$ >80 GBq/μmol, $n = 2$). It is also our interest to evaluate brain permeability of **33** ([^{11}C]**18**), which was synthesized from [^{11}C]COCl$_2$ in 13% decay-corrected RCY based on starting [^{11}C]CO$_2$ at end-of-synthesis with >99% radiochemical purity ($n = 1$). In summary, all these radioligands showed no signs of radiolysis up to 90 min after formulation. The efficient radiosynthesis with high radiochemical purity and molar activities of **30**—**33** enabled the subsequent *in vitro* and *in vivo* evaluation.

2.6. Preliminary PET imaging studies in rat brain

Dynamic PET acquisitions were carried out with **30**—**33** in Sprague-Dawley rats for 60 min. Representative PET images of **32** (sagittal and coronal, summed images 0—60 min) and time-activity

Table 1
Physicochemical properties of compounds **3**, **17**—**19** and **21**.

Entry	3	17	18	19	21
LogD[a]	2.13 ± 0.04	2.17 ± 0.07	2.67 ± 0.23	2.01 ± 0.20	3.18 ± 0.31
tPSA[b]	64.9	50.3	50.3	50.3	50.3
MPO[c]	5.2	4.0	3.7	3.7	3.9

[a] Distribution coefficient (LogD) was measured by the 'shake-flask' method and quantified by LC-MS. The data are expressed in mean ± SD (n = 3).
[b] Topological polar surface area (tPSA) was calculated by ChemBioDraw Ultra 14.0.
[c] MPO score was calculated using the method reported in Zhang, L.*et al.* [63].

A. Radiosynthesis of tracer 30
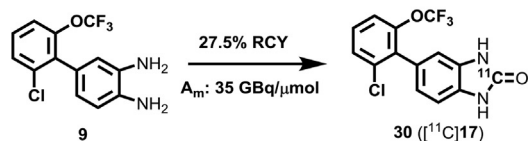
B. Radiosynthesis of tracer 31
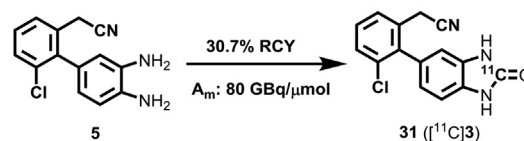
C. Radiosynthesis of tracer 32
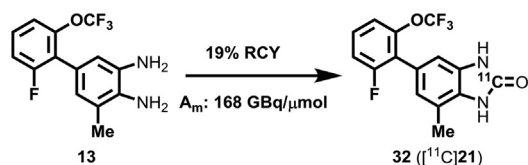
D. Radiosynthesis of tracer 33
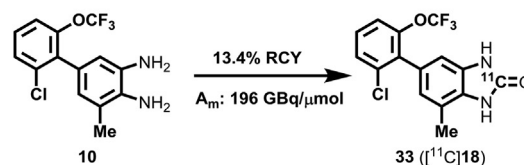
Scheme 2. Radiolabeling of tracers **30**–**33**. Conditions: [^{11}C]COCl$_2$, Et$_3$N, THF; 30 °C, 1 min.

curves of two characteristic brain regions, namely TARP γ-8 enriched hippocampus and TARP γ-8 deficient cerebellum, are shown in Fig. 6. Time-activity curves of **30**, **32**, **33** in the whole brain are shown in Fig. S2, Supporting Information. Compounds **30**, **32** and **33** all demonstrated reasonable blood-brain-barrier (BBB) penetration ability with maximum standard uptake value (SUV) of ca. 1.0, 0.8 and 0.8 in the whole brain, respectively. The regional distribution of **32** was heterogeneous with high uptake observed in the hippocampus and low uptake in the cerebellum (Fig. 6A and B), consistent with TARP γ-8 expression in the rodent brain [68]. **30**

A. Representative PET images of tracer 32
(0-60 min summed image, baseline)
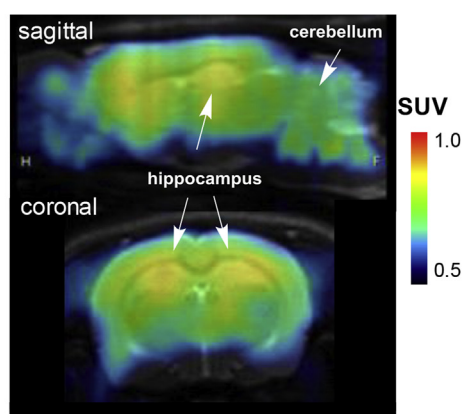
B. Time-activity curves of tracer 32
(baseline)
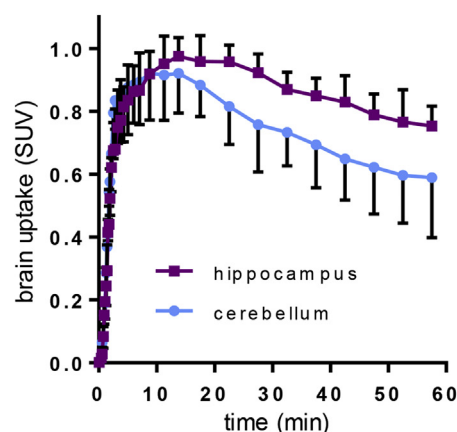
C. Time-activity curves of tracer 30
(baseline)
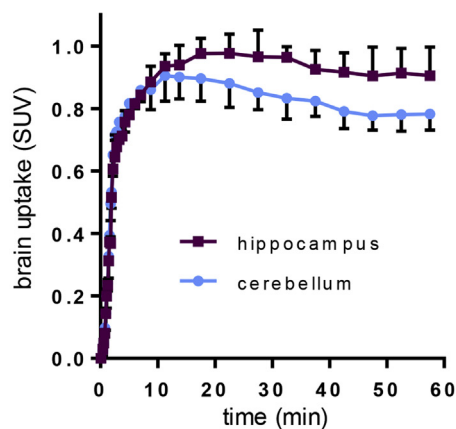
D. PET images of 31
(0-60 min summed)
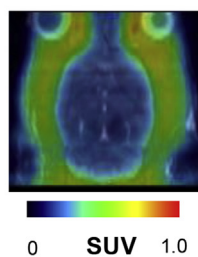
E. Time-activity curves of 31
(whole brain)
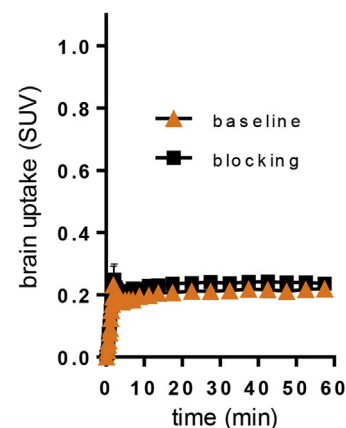
Fig. 6. Representative PET images and time-activity curves of **30**–**32** in rat brain: (A) baseline PET images (summed 0–60 min) of **32**; (B and C) time-activity curve of **32** and **30** under baseline in the region of hippocampus (high expression) and cerebellum (low expression); (D) baseline PET images (summed 0–60 min) of **31** and (E) whole brain time-activity curve of **31** under baseline and blocking conditions (1 mg/kg, JNJ56022486).

also showed a similar distribution pattern as shown in Fig. 6C. However, pretreatment of **32** with unlabeled **21** (1 mg/kg) or **30** with JNJ5551118 (1 mg/kg) failed to show significant reduction of brain uptake, probably attributed to *in vivo* nonspecific binding (Fig. S2). Compound **31** showed limited whole brain uptake (ca. 0.2 SUV), which might cause no significant changes between baseline and blocking conditions (JNJ56022486, 1 mg/kg, Fig. 6D and E).
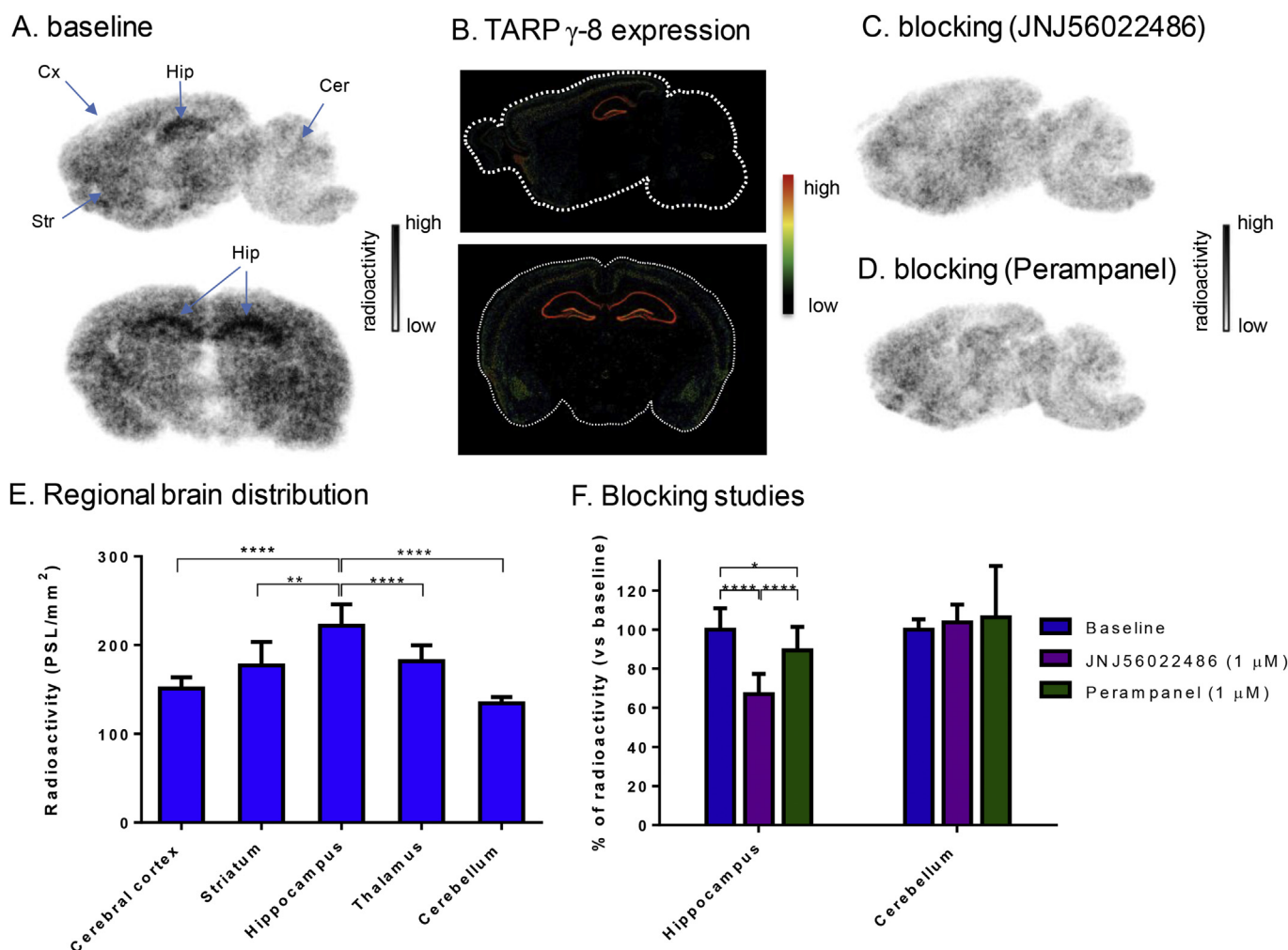
2.7. In vitro autoradiography

Since structural scaffolds bearing **30** and **32** showed a high level of nonspecific binding *in vivo*, we shifted our focus into a structurally diverse molecule **31**. The *in vitro* binding specificity of **31** was evaluated by *in vitro* autoradiography studies. Representative *in vitro* autoradiograms of **31** on sagittal and coronal sections of rat brains are shown in Fig. 7A. The baseline study demonstrated the heterogeneous distribution of bound radioactivity with signal levels from high to low in the order of hippocampus, striatum, thalamus, cerebral cortex and cerebellum (Fig. 7A and D). The distribution pattern was consistent with the mRNA expression pattern of TARP γ-8 with the highest signal level in the region of the hippocampus and the lowest level in the cerebellum (Fig. 7B). Blocking studies with JNJ56022486 (1 μM) resulted in greater than

30% reduction of the bound radioactivity in hippocampus and abolishment of the heterogeneity in different brain regions. No notable change was observed for the reference region, *i.e.*, the cerebellum (Fig. 7C and E). These results indicated that **31** had a reasonable medium-to-good level of *in vitro* specific binding to AMPARs complexed with TARP γ-8.

2.8. Efflux transporter inhibition experiments

Since **31** showed promising *in vitro* binding specificity towards TARP γ-8 dependent AMPARs, we next investigated the underlying cause of low brain uptake. Recent studies demonstrated that both P-glycoprotein (Pgp) and breast cancer resistance protein (Bcrp) are essential members of the ABC transporter family, which co-localize at the BBB [69]. Many drug molecules, which are substrates of Pgp and/or Bcrp, are promptly excreted back into the blood from the brain and thus exhibit limited brain uptake. To determine whether the low uptake is attributed to the excretion from the brain by the Pgp and/or Bcrp, we performed *ex vivo* measurement of **31** brain uptake under the administration of tariquidar (TQD), a Pgp inhibitor, and/or Ko143, a Bcrp inhibitor [70]. TQD (8 mg/kg) or the combination of TQD (8 mg/kg) and Ko143 (15 mg/kg) was administrated intravenously via tail vein 2 h (for TQD) or 1 h (for Ko143)

Fig. 7. *In vitro* autoradiography of **31** binding in rat brain sections. (A) Brain sections were treated with **31**; (B) TARP γ-8 mRNA expression. Data were retrieved from mouse.brain-map.org, experiment# 70724625 and 72108823; (C) Brain sections were treated with **31** in the presence of JNJ56022486 (1 μM); (D) The radioactivity distribution was quantified in regional rat brain (baseline). The data are expressed as radioactivity per mm^2 (n = 4) and (E) Blocking studies. The data are normalized to % of radioactivity vs control (n = 4). Cer, cerebellum; Hip, hippocampus; Cx, cortex; Str, striatum. Asterisks indicate statistical significance. $^*p < 0.05$, $^{**}p < 0.01$, and $^{****}p < 0.0001$ vs control.
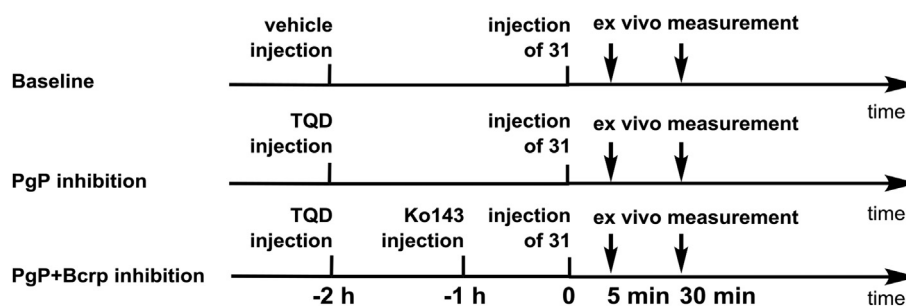
Scheme 3. Brain efflux transporter inhibition experiments.

before injection of **31** (Scheme 3). The brain uptake was measured at 5 min and 30 min post-injection under control and PgP/Bcrp inhibition conditions. As depicted in Table 2, TQD pretreatment increased the brain uptake to 146% and 204% at 5 min and 30 min post-injection, respectively. The more profound effect was observed when PgP/Bcrp were simultaneously inhibited by TQD

and Ko143, which showed 186% and 282% increased brain uptake. The brain-to-blood ratio also increased significantly under Pgp (177% and 206% at 5 and 30 min post injection, respectively) and Pgp/Bcrp (202% and 233% at 5 and 30 min post injection, respectively) inhibition conditions, the trend of which was consistent with the observations in the brain uptake (Table 2). These findings

Table 2
Effect of tariquidar (TQD) and Ko143 on brain uptake of **31** and brain-to-blood ratio in mice.

(A) brain uptake under baseline and PgP inhibition conditions				%increase under PgP inhibition	%increase under PgP/Bcrp inhibition
Time	Brain uptake (%ID/g)[a]				
	Control	TQD[b]	TQD + Ko143[b,c]		
5min[d]	0.50 ± 0.10	0.73 ± 0.12	0.93 ± 0.18	146 ± 23*	186 ± 36**
30 min[e]	0.71 ± 0.08	1.46 ± 0.19	2.02 ± 0.51	204 ± 27****	282 ± 73**

(B) brain-to-blood ratio under baseline and PgP inhibition conditions				%increase under PgP inhibition	%increase under PgP/Bcrp inhibition
Time	Brain uptake (%ID/g)[a]				
	Control	TQD[b]	TQD + Ko143[b,c]		
5min[d]	0.19 ± 0.05	0.34 ± 0.05	0.38 ± 0.05	177 ± 26**	202 ± 27**
30 min[e]	0.35 ± 0.01	0.72 ± 0.43	0.83 ± 0.12	206 ± 110*	233 ± 34***

Asterisks indicate statistical significance. $^*p < 0.05$ vs control. $^{**}p < 0.01$ vs control. $^{***}p < 0.0004$ vs control. $^{****}p < 0.0001$ vs control.
[a] The data are expressed in mean ± SD (n = 3−4).
[b] TQD (8 mg/kg) was intravenously injected into mice 2 h before tracer injection.
[c] Ko143 (15 mg/kg) was intravenously injected into mice 1 h before tracer injection.
[d] Tracer uptake was expressed as %ID/g 5 min post-injection of **31**.
[e] Tracer uptake was expressed as %ID/g 30 min post-injection of **31**.
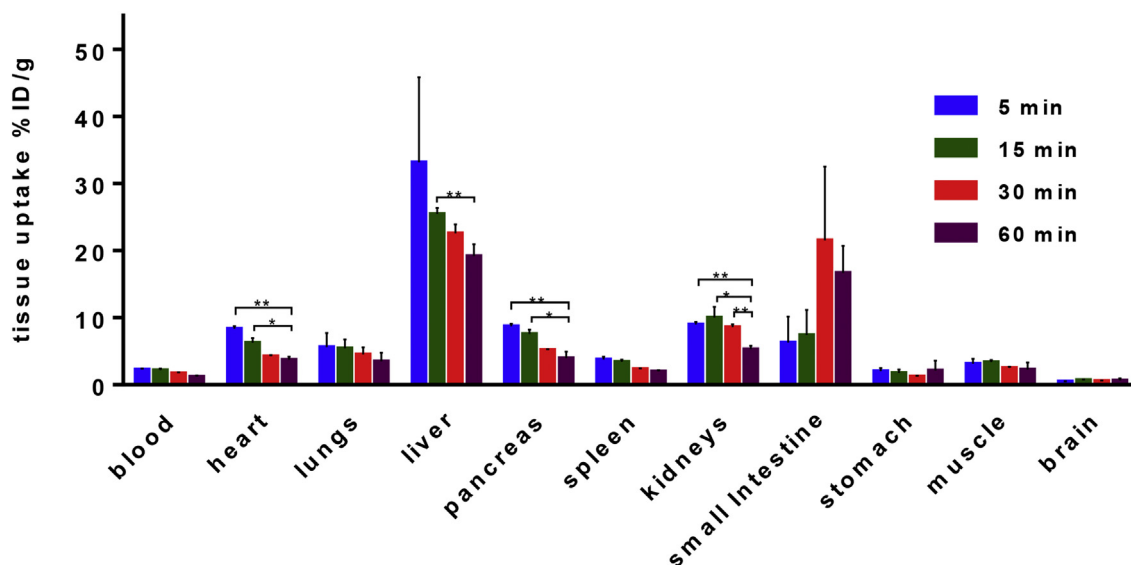
Fig. 8. *Ex vivo* biodistribution in mice at four different time points (5, 15, 30 and 60 min) post injection of **31**. All data are mean ± SD, n = 4. Asterisks indicate statistical significance. $^*p < 0.05$, and $^{**}p \leq 0.01$.

suggested that **31** had intensive interactions with brain efflux pumps including Pgp and Bcrp at the BBB, which may, in part, account for the low brain accumulation of **31** at tracer dose.

2.9. Whole body ex vivo biodistribution studies and radiometabolite analysis

The uptake, biodistribution and clearance of **31** were investigated in mice at four time points (5, 15, 30 and 60 min) after i.v. injection of the radiotracer (Fig. 8 and Table S1, Supporting Information). Several organs including heart, lungs, pancreas, small intestine, kidneys and liver exhibited high uptake (>5% ID/g) at 5 min post-injection. After the initial uptake, the radioactivity in heart, lungs, pancreas and liver decreased rapidly, while that in small intestine and kidney started to decrease at 15 and 30 min post-injection, respectively. These results together with high radioactivity remaining in liver, kidneys and small intestine at 60 min post-injection demonstrated the rapid hepatobiliary elimination of **31**, and concurrently relatively-slow urinary elimination. To evaluate the stability of **31** in vivo, radiometabolites in the plasma and brain homogenate in mice were evaluated at 30 min post-injection of the radiotracer. The fraction of unchanged **31** in brain and plasma was determined to be 65% and 35%, respectively, and SMARTCyp [71] was utilized to propose three possible sites for the metabolism (Table S2 in the supporting information). These results indicated that **31** showed reasonable stability in the brain and relatively rapid metabolism in the plasma.

3. Conclusion

We have efficiently synthesized a focused library of AMPAR/TARP γ-8 antagonists containing 1,3-dihydro-2*H*-benzo [*d*]imidazole-2-ones and benzo [*d*]thiazol-2(3*H*)-ones. IC$_{50}$ values towards TARP γ-8 and subtype-selectivity between TARP γ-2 and TARP γ-8 were determined in vitro by calcium flux assay on human HEK-293 cells expressing AMPA GluA1 + TARP γ-8. Physiochemical properties including distribution coefficient (Log*D*), and in silico MPO and tPSA values were also measured. As a result, compounds **3, 17**−**19** and **21** were identified as promising candidates for the PET tracer development. ^{11}C-Carbonylation labeling strategy using [^{11}C]COCl$_2$ was employed to provide [^{11}C-carbonyl] labeled TARP γ-8 dependent AMPAR antagonists in high radiochemical yield (13−31%), high molar activity (35−196 GBq/μmol) and high radiochemical purity (>99%). The pharmacokinetic profile including brain uptake, clearance and binding specificity of compounds **30**−**32** was evaluated by PET. While trifluoromethoxy substituted tracers **30** and **32** showed heterogenous regional brain uptake, which was consistent with TARP γ-8 distribution, further investigation was not pursued due to high nonspecific binding evidenced in the blocking experiment. To our delight, despite low brain uptake in PET experiments, a structurally diverse tracer **31** demonstrated good in vitro specific binding and heterogeneous regional brain uptake, which was aligned with TARP γ-8 distribution. We also carried out efflux transporter inhibition experiments to confirm the underlying reason for low brain uptake of **31**, which was, to a large extent, attributed to the PgP/Bcrp efflux mechanism. Further optimization to improve the brain uptake and minimize the intensive interaction with PgP/Bcrp is needed. As a result, this work not only represents the first medicinal chemistry approach towards subtype selective AMPAR PET tracers, but also offers a new roadmap towards next generation AMPAR tracers by utilizing the knowledge of pharmacology, molecular docking, physiochemical properties as well as radiochemistry presented in this work.

Author contributions

The manuscript was written through contributions of all authors. All authors have given approval to the final version of the manuscript. #Z. Chen and W. Mori contributed equally.

Notes

The authors declare no competing financial interest.

Acknowledgements

Appendix A. Supplementary data

Supplementary data related to this article can be found at https://doi.org/10.1016/j.ejmech.2018.08.019.

References

[1] B.S. Meldrum, Glutamate as a neurotransmitter in the brain: review of physiology and pathology, J. Nutr. 130 (2000) 1007S–1015S.

[2] J.C. Watkins, D.E. Jane, The glutamate story, Br. J. Pharmacol. 147 (2006) S100–S108.

[3] R. Dingledine, K. Borges, D. Bowie, S.F. Traynelis, The glutamate receptor ion channels, Pharmacol. Rev. 51 (1999) 7–61.

[4] M.L. Mayer, N. Armstrong, Structure and function of glutamate receptor ion channels, Annu. Rev. Physiol. 66 (2004) 161–181.

[5] S.F. Traynelis, L.P. Wollmuth, C.J. McBain, F.S. Menniti, K.M. Vance, K.K. Ogden, K.B. Hansen, H.J. Yuan, S.J. Myers, R. Dingledine, Glutamate receptor ion channels: structure, regulation, and function, Pharmacol. Rev. 62 (2010) 405–496.

[6] M. Hollmann, S. Heinemann, Cloned glutamate receptors, Annu. Rev. Neurosci. 17 (1994) 31–108.

[7] B. Compans, D. Choquet, E. Hosy, Review on the role of AMPA receptor nanoorganization and dynamic in the properties of synaptic transmission, Neurophotonics 3 (2016) 041811.

[8] P. Calabresi, L.M. Cupini, D. Centonze, F. Pisani, G. Bernardi, Antiepileptic drugs as a possible neuroprotective strategy in brain ischemia, Ann. Neurol. 53 (2003) 693–702.

[9] P.K. Chang, D. Verbich, R.A. McKinney, AMPA receptors as drug targets in neurological disease-advantages, caveats, and future outlook, Eur. J. Neurosci. 35 (2012) 1908–1916.

[10] L. Turski, A. Huth, M. Sheardown, F. McDonald, R. Neuhaus, H.H. Schneider, U. Dirnagl, F. Wiegand, P. Jacobsen, E. Ottow, ZK200775: a phosphonate quinoxalinedione AMPA antagonist for neuroprotection in stroke and trauma, Proc. Natl. Acad. Sci. U.S.A. 95 (1998) 10960–10965.

[11] P.L. Ornstein, M.B. Arnold, N.K. Augenstein, D. Lodge, J.D. Leander, D.D. Schoepp, (3SR,4aRS,6RS,8aRS)-6-[2-(1*H*-tetrazol-5-yl)ethyl]decahydroisoquinoline-3-carboxylic acid: a structurally novel, systemically active, competitive AMPA receptor antagonist, J. Med. Chem. 36 (1993) 2046–2048.

[12] I. Gilron, M.B. Max, G. Lee, S.L. Booher, C.N. Sang, A.S. Chappell, R.A. Dionne, Effects of the 2-amino-3-hydroxy-5-methyl-4-isoxazole-proprionic acid/kainate antagonist LY293558 on spontaneous and evoked postoperative pain, Clin. Pharmacol. Ther. 68 (2000) 320–327.

[13] E. Faught, BGG492 (selurampanel), an AMPA/kainate receptor antagonist drug for epilepsy, Expet Opin. Invest. Drugs 23 (2014) 107–113.

[14] A.S. Chappell, J.W. Sander, M.J. Brodie, D. Chadwick, A. Lledo, D. Zhang, J. Bjerke, G.M. Kiesler, S. Arroyo, A crossover, add-on trial of talampanel in patients with refractory partial seizures, Neurology 58 (2002) 1680–1682.

[15] V. Feigin, Irampanel boehringer ingelheim, Curr. Opin. Invest. Drugs 3 (2002) 908–910.

[16] J.A. French, G.L. Krauss, B.J. Steinhoff, D. Squillacote, H. Yang, D. Kumar, A. Laurenza, Evaluation of adjunctive perampanel in patients with refractory partial-onset seizures: results of randomized global phase III study 305, Epilepsia 54 (2013) 117–125.

[17] R. Zwart, E. Sher, X. Ping, X. Jin, J.R. Sims, A.S. Chappell, S.D. Gleason, P.J. Hahn, K. Gardinier, D.L. Gernert, J. Hobbs, J.L. Smith, S.N. Valli, J.M. Witkin,

Perampanel, an antagonist of α-amino-3-hydroxy-5-methyl-4-isoxazolepropionic acid receptors, for the treatment of epilepsy: studies in human epileptic brain and nonepileptic brain and in rodent models, J. Pharmacol. Exp. Therapeut. 351 (2014) 124–133.

[18] D. Ko, H. Yang, B. Williams, D. Xing, A. Laurenza, Perampanel in the treatment of partial seizures: time to onset and duration of most common adverse events from pooled Phase III and extension studies, Epilepsy Behav. 48 (2015) 45–52.

[19] V.A. Letts, R. Felix, G.H. Biddlecome, J. Arikkath, C.L. Mahaffey, A. Valenzuela, F.S. Bartlett, Y. Mori, K.P. Campbell, W.N. Frankel, The mouse stargazer gene encodes a neuronal Ca^{2+}-channel gamma subunit, Nat. Genet. 19 (1998) 340–347.

[20] D.L. Burgess, C.F. Davis, L.A. Gefrides, J.L. Noebels, Identification of three novel Ca^{2+} channel gamma subunit genes reveals molecular diversification by tandem and chromosome duplication, Genome Res. 9 (1999) 1204–1213.

[21] N. Klugbauer, S. Dai, V. Specht, L. Lacinová, E. Marais, G. Bohn, F. Hofmann, A family of gamma-like calcium channel subunits, FEBS Lett. 470 (2000) 189–197.

[22] A.S. Shaw, E.L. Filbert, Scaffold proteins and immune-cell signalling, Nat. Rev. Immunol. 9 (2009) 47–56.

[23] D. Yan, S. Tomita, Defined criteria for auxiliary subunits of glutamate receptors, J. Physiol. 590 (2012) 21–31.

[24] A.C. Jackson, R.A. Nicoll, The expanding social network of ionotropic glutamate receptors: TARPs and other transmembrane auxiliary subunits, Neuron 70 (2011) 178–199.

[25] K. Hashimoto, M. Fukaya, X. Qiao, K. Sakimura, M. Watanabe, M. Kano, Impairment of AMPA receptor function in cerebellar granule cells of ataxic mutant mouse stargazer, J. Neurosci. 19 (1999) 6027–6036.

[26] S. Tomita, Regulation of ionotropic glutamate receptors by their auxiliary subunits, Physiology 25 (2010) 41–49.

[27] A.C. Jackson, R.A. Nicoll, The expanding social network of ionotropic glutamate receptors: TARPs and other transmembrane auxiliary subunits, Neuron 70 (2011) 178–199.

[28] S. Tomita, L. Chen, Y. Kawasaki, R.S. Petralia, R.J. Wenthold, R.A. Nicoll, D.S. Bredt, Functional studies and distribution define a family of transmembrane AMPA receptor regulatory proteins, J. Cell Biol. 161 (2003) 805–816.

[29] M. Fukaya, M. Yamazaki, K. Sakimura, M. Watanabe, Spatial diversity in gene expression for VDCCγ subunit family in developing and adult mouse brains, Neurosci. Res. 53 (2005) 376–383.

[30] M.B. Gill, D.S. Bredt, An emerging role for TARPs in neuropsychiatric disorders, Neuropsychopharmacology 36 (2011) 362–363.

[31] N. Rouach, K. Byrd, R.S. Petralia, G.M. Elias, H. Adesnik, S. Tomita, S. Karimzadegan, C. Kealey, D.S. Bredt, R.A. Nicoll, TARP γ-8 controls hippocampal AMPA receptor number, distribution and synaptic plasticity, Nat. Neurosci. 8 (2005) 1525–1533.

[32] M. Fukaya, M. Tsujita, M. Yamazaki, E. Kushiya, M. Abe, K. Akashi, R. Natsume, M. Kano, H. Kamiya, M. Watanabe, K. Sakimura, Abundant distribution of TARP γ-8 in synaptic and extrasynaptic surface of hippocampal neurons and its major role in AMPA receptor expression on spines and dendrites, Eur. J. Neurosci. 24 (2006) 2177–2190.

[33] S.D. Gleason, A. Kato, H.H. Bui, L.K. Thompson, S.N. Valli, P.V. Stutz, M.-S. Kuo, J.F. Falcone, W.H. Anderson, X. Li, J.M. Witkin, Inquiries into the biological significance of transmembrane AMPA receptor regulatory protein (TARP) γ–8 through investigations of TARP γ–8 Null Mice, CNS Neurol. Disord. - Drug Targets 14 (2015) 612–626.

[34] M. Yamasaki, M. Fukaya, M. Yamazaki, H. Azechi, R. Natsume, M. Abe, K. Sakimura, X. Watanabe, TARP γ-2 and γ-8 differentially control AMPAR density across schaffer collateral/commissural synapses in the hippocampal CA1 area, J. Neurosci. 36 (2016) 4296–4312.

[35] M.P. Maher, N. Wu, S. Ravula, M.K. Ameriks, B.M. Savall, C. Liu, B. Lord, R.M. Wyatt, J.A. Matta, C. Dugovic, S. Yun, L.V. Donck, T. Steckler, A.D. Wickenden, N.I. Carruthers, T.W. Lovenberg, Discovery and characterization of AMPA receptor modulators selective for TARP-γ8, J. Pharmacol. Exp. Therapeut. 357 (2016) 394–414.

[36] K.M. Gardinier, D.L. Gernert, W.J. Porter, J.K. Reel, P.L. Ornstein, P. Spinazze, F.C. Stevens, P. Hahn, S.P. Hollinshead, D. Mayhugh, J. Schkeryantz, A. Khilevich, O.D. Frutos, S.D. Gleason, A.S. Kato, D. Luffer-Atlas, P.V. Desai, S. Swanson, K.D. Burris, C. Ding, B.A. Heinz, A.B. Need, V.N. Barth, G.A. Stephenson, B.A. Diseroad, T.A. Woods, H.Y.D. Bredt, J.M. Witkin, Discovery of the first α-amino-3-hydroxy-5-methyl-4-isoxazolepropionic acid (AMPA) receptor antagonist dependent upon transmembrane AMPA receptor regulatory protein (TARP) γ-8, J. Med. Chem. 59 (2016) 4753–4768.

[37] M.R. Lee, K.M. Gardinier, D.L. Gernert, D.A. Schober, R.A. Wright, H. Wang, Y. Qian, J.M. Witkin, E.S. Nisenbaum, A.S. Kato, Structural determinants of the γ-8 TARP dependent AMPA receptor antagonist, ACS Chem. Neurosci. 8 (2017) 2631–2647.

[38] J.M. Witkin, J. Li, G. Gilmour, S.N. Mitchell, G. Carter, S.D. Gleason, W.F. Seidel, B.J. Eastwood, A. McCarthy, W.J. Porter, J. Reel, K.M. Gardinier, A.S. Kato, K.A. Wafford, Electroencephalographic, cognitive, and neurochemical effects of LY3130481 (CERC-611), a selective antagonist of TARP-γ8-associated AMPA receptors, Neuropharmacology 126 (2017) 257–270.

[39] M.E. Phelps, Positron emission tomography provides molecular imaging of biological processes, Proc. Natl. Acad. Sci. Unit. States Am. 97 (2000) 9226–9233.

[40] C.M. Lee, L. Farde, Using positron emission tomography to facilitate CNS drug development, Trends Pharmacol. Sci. 27 (2006) 310–316.

[41] J.K. Willmann, N.v. Bruggen, L.M. Dinkelborg, S.S. Gambhir, Molecular imaging in drug development, Nat. Rev. Drug Discov. 7 (2008) 591–607.

[42] M. Gao, D. Kong, A. Clearfield, Q.-H. Zheng, Synthesis of carbon-11 and fluorine-18 labeled N-acetyl-1-aryl-6,7-dimethoxy-1,2,3,4-tetrahydroisoquinoline derivatives as new potential PET AMPA receptor ligands, Bioorg. Med. Chem. Lett 16 (2006) 2229–2233.

[43] E. Årstad, R. Gitto, A. Chimirri, R. Caruso, A. Constanti, D. Turton, S.P. Hume, R. Ahmad, L.S. Pilowskyd, S.K. Luthra, Closing in on the AMPA receptor: synthesis and evaluation of 2-acetyl-1-(40-chlorophenyl)-6-methoxy-7-[^{11}C]methoxy-1,2,3,4-tetrahydroisoquinoline as a potential PET tracer, Bioorg. Med. Chem. 14 (2006) 4712–4717.

[44] U.B. Kronenberg, B. Drewes, W. Sihver, H.H. Coenen, N-2-(4-N-(4-[^{18}F]Fluorobenzamido)phenyl)-propyl-2-propanesulphonamide: synthesis and radiofluorination of a putative AMPA receptor ligand, J. Label. Compd. Radiopharm. 50 (2007) 1169–1175.

[45] H.G. Lee, P.J. Milner, M.S. Placzek, S.L. Buchwald, J.M. Hooker, Virtually instantaneous, room-temperature [^{11}C]-cyanation using biaryl phosphine Pd(0) complexes, J. Am. Chem. Soc. 137 (2015) 648–651.

[46] N. Oi, M. Tokunaga, M. Suzuki, Y. Nagai, Y. Nakatani, N. Yamamoto, J. Maeda, T. Minamimoto, M.-R. Zhang, T. Suhara, M. Higuchi, Development of novel PET probes for central 2-amino-3-(3-hydroxy-5-methyl-4-isoxazolyl)propionic acid receptors, J. Med. Chem. 58 (2015) 8444–8462.

[47] K. Takahata, Y. Kimura, C. Seki, M. Tokunaga, M. Ichise, K. Kawamura, M. Ono, S. Kitamura, M. Kubota, S. Moriguchi, T. Ishii, Y. Takado, F. Niwa, H. Endo, T. Nagashima, Y. Ikoma, M.-R. Zhang, T. Suhara, M. Higuchi, A human PET study of [11C]HMS011, a potential radioligand for AMPA receptors, EJNMMI Res. 7 (2017) 63.

[48] G. Yuan, G.B. Jones, N. Vasdev, S.H. Liang, Radiosynthesis and preliminary PET evaluation of 18F-labeled 2-(1-(3-fluorophenyl)-2-oxo-5-(pyrimidin-2-yl)-1,2-dihydropyridin-3-yl) benzonitrile for imaging AMPA receptors, Bioorg. Med. Chem. Lett 26 (2016) 4857–4860.

[49] Y. Zhao, S. Chen, C. Yoshioka, I. Baconguis, E. Gouaux, Architecture of fully occupied GluA2 AMPA receptor-TARP complex elucidated by cryo-EM, Nature 536 (2016) 108–111.

[50] E.C. Twomey, M.V. Yelshanskaya, R.A. Grassucci, J. Frank, A.I. Sobolevsky, Elucidation of AMPA receptor-stargazin complexes by cryo-electron microscopy, Science 353 (2016) 83–86.

[51] O. Trott, A.J. Olson, AutoDock Vina, Improving the speed and accuracy of docking with a new scoring function, efficient optimization, and multi-threading, J. Comput. Chem. 31 (2010) 455–461.

[52] A.S. Kato, M.B. Gill, H. Yu, E.S. Nisenbaum, D.S. Bredt, TARPs differentially decorate AMPA receptors to specify neuropharmacology, Trends Neurosci. 33 (2010) 241–248.

[53] P.J. Chu, H.M. Robertson, P.M. Best, Calcium channel gamma subunits provide insights into the evolution of this gene family, Gene 280 (2001) 37–48.

[54] A.S. Kato, E.R. Siuda, E.S. Nisenbaum, D.S. Bredt, AMPA receptor subunit-specific regulation by a distinct family of type II TARPs, Neuron 59 (2008) 986–996.

[55] S. Tomita, H. Adesnik, M. Sekiguchi, W. Zhang, K. Wada, J.R. Howe, R.A. Nicoll, D.S. Bredt, Stargazin modulates AMPA receptor gating and trafficking by distinct domains, Nature 435 (2005) 1052–1058.

[56] I. Riva, C. Eibl, R. Volkmer, A.L. Carbone, A.J. Plested, Control of AMPA receptor activity by the extracellular loops of auxiliary proteins, eLife 6 (2017) e28680.

[57] S. Chen, Y. Zhao, Y. Wang, M. Shekhar, E. Tajkhorshid, E. Gouaux, Activation and desensitization mechanism of AMPA receptor-TARP complex by cryo-EM, Cell 170 (2017) 1234–1246.

[58] S. Tomita, A. Shenoy, Y. Fukata, R.A. Nicoll, D.S. Bredt, Stargazin interacts functionally with the AMPA receptor glutamate-binding module, Neuro-pharmacology 52 (2007) 87–91.

[59] R.N. Waterhouse, Determination of lipophilicity and its use as a predictor of blood-brain barrier penetration of molecular imaging agents, Mol. Imag. Biol. 5 (2003) 376–389.

[60] S. Patel, R. Gibson, In vivo site-directed radiotracers: a mini-review, Nucl. Med. Biol. 35 (2008) 805–815.

[61] V.W. Pike, Considerations in the development of reversibly binding PET radioligands for brain imaging, Curr. Med. Chem. 23 (2016) 1818–1869.

[62] OECD, Test No. 107: Partition Coefficient (N-octanol/water): Shake Flask Method, OECD Publishing.

[63] L. Zhang, A. Villalobos, E.M. Beck, T. Bocan, T.A. Chappie, L. Chen, S. Grimwood, S.D. Heck, C.J. Helal, X. Hou, J.M. Humphrey, J. Lu, M.B. Skaddan, T.J. McCarthy, P.R. Verhoest, T.T. Wager, K. Zasadny, Design and selection parameters to accelerate the discovery of novel central nervous system positron emission tomography (PET) ligands and their application in the development of a novel phosphodiesterase 2A PET ligand, J. Med. Chem. 56 (2013) 4568–4579.

[64] B.H. Rotstein, S.H. Liang, M.S. Placzek, J.M. Hooker, A.D. Gee, F. Dolle, A.A. Wilson, N. Vasdev, ^{11}C=O bonds made easily for positron emission tomography radiopharmaceuticals, Chem. Soc. Rev. 45 (2016) 4708–4726.

[65] G. Roger, B. Lagnel, L. Besret, Y. Bramoulle, C. Coulon, M. Ottaviani, M. Kassiou, M. Bottlaender, H. Valette, F. Dolle, Synthesis, radiosynthesis and in vivo evaluation of 5-[3-(4-benzylpiperidin-1-yl)prop-1-ynyl]-1,3-dihydrobenzoimidazol-2-[(11)C]one, as a potent NR(1A)/2B subtype selective NMDA PET radiotracer, Bioorg. Med. Chem. 11 (2003) 5401–5408.

[66] G. Roger, F. Dolle, B. De Bruin, X. Liu, L. Besret, Y. Bramoulle, C. Coulon,

M. Ottaviani, M. Bottlaender, H. Valette, M. Kassiou, Radiosynthesis and pharmacological evaluation of [11C]EMD-95885: a high affinity ligand for NR2B-containing NMDA receptors, Bioorg. Med. Chem. 12 (2004) 3229–3237.

[67] L. Wang, W. Mori, R. Cheng, J. Yui, A. Hatori, L. Ma, Y. Zhang, B.H. Rotstein, M. Fujinaga, Y. Shimoda, T. Yamasaki, L. Xie, Y. Nagai, T. Minamimoto, M. Higuchi, N. Vasdev, M.-R. Zhang, S.H. Liang, Synthesis and preclinical evaluation of sulfonamido-based [^{11}C-*Carbonyl*]-carbamates and ureas for imaging monoacylglycerol lipase, Theranostics 6 (2016) 1145–1159.

[68] M.R. Lee, K.M. Gardinier, D.L. Gernert, D.A. Schober, R.A. Wright, H. Wang, Y. Qian, J.M. Witkin, E.S. Nisenbaum, A.S. Kato, Structural determinants of the gamma-8 TARP dependent AMPA receptor antagonist, ACS Chem. Neurosci. 8 (2017) 2631–2647.

[69] T. Tatsuta, M. Naito, T. Oh-hara, I. Sugawara, T. Tsuruo, Functional involvement of P-glycoprotein in blood-brain barrier, J. Biol. Chem. 267 (1992) 20383–20391.

[70] T. Wanek, C. Kuntner, J.P. Bankstahl, S. Mairinger, M. Bankstahl, J. Stanek, M. Sauberer, T. Filip, T. Erker, M. Muller, W. Loscher, O. Langer, A novel PET protocol for visualization of breast cancer resistance protein function at the blood-brain barrier, J. Cerebr. Blood Flow Metabol. 32 (2012) 2002–2011.

[71] P. Rydberg, D.E. Gloriam, J. Zaretzki, C. Breneman, L. Olsen, SMARTCyp: a 2D method for prediction of cytochrome P450-Mediated drug metabolism, ACS Med. Chem. Lett. 1 (2010) 96–100.